https://doi.org/10.1016/j.renene.2020.02.050

The effect of urban morphology on the solar capacity of three-dimensional cities

Rui Zhu[a,b], Man Sing Wong[b,*], Linlin You[a], Paolo Santi[c,d], Janet Nichol[e], Hung Chak Ho[f], Lin Lu[g], Carlo Ratti[c]

[a] *Future Urban Mobility, Singapore-MIT Alliance for Research and Technology, 1 Create Way, #09-02 Create Tower, Singapore 138062*
[b] *Department of Land Surveying and Geo-Informatics, The Hong Kong Polytechnic University, ZS616, 181 Chatham Road South, Kowloon, Hong Kong*
[c] *Senseable City Laboratory, Massachusetts Institute of Technology, Cambridge MA 02139 USA*
[d] *Istituto di Informatica e Telematica del CNR, 56124 Pisa, Italy*
[e] *Department of Geography, University of Sussex, United Kingdom*
[f] *Department of Urban Planning and Design, The University of Hong Kong, 831 Knowles Building, Pok Fu Lam, Hong Kong*
[g] *Department of Building Services Engineering, The Hong Kong Polytechnic University, ZS850, 181 Chatham Road South, Kowloon, Hong Kong*

Abstract

As a clean and renewable resource, solar energy is increasingly being used to relieve the pressures on environmental protection and the exhaustion of conventional energy. Although photovoltaic cells have been installed in many cities, the lack of quantitative mapping of the annual solar energy potential of urban surfaces hinders the effective utilization of solar energy, since different urban morphologies may result in radically different amounts of solar radiation being received. Herein, we provide solar irradiation estimation solution for three-dimensional (3D) cities to carefully quantify the distribution of the annual irradiations of urban surfaces and to investigate the effect of urban morphology on the resulting solar capacity, having accounted for weather effects. By modeling urban surfaces as 3D point clouds, annual irradiations of the point clouds have been estimated, accompanied by the creation of shadows on the ground, rooftops, and wall façades. An empirical investigation across ten cities suggests that urban areas at lower latitudes tend to have larger annual irradiations, although weather may affect this trend; moreover, an area having greater building heights consistently has the largest third quartile of irradiation compared with an area having lower buildings in the same city. Conversely, areas with a majority of low buildings have a more significant proportion of usable areas; in this arrangement, façades can optimally utilize solar energy as large irradiations are concentrated on particular façades. The Pearson correlation coefficients between solar capacity and relevant urban morphology indices are strong and positive. Additionally, cities in higher latitudes tend to have a larger solar capacity, but the density of building footprints has a negative effect on solar capacity when it becomes notably large. These findings suggest that urban morphology has an essential effect on solar capacity, and our results enable the determination of favorable solar cities.

Keywords: Solar energy; 3D solar cities; Solar capacity; Urban morphology

1. Introduction

Presently, pressures from the exhaustion of conventional energy (e.g., fossil fuels) and environmental pollution promote wider adoption of renewable energies [1]. As a readily available source of renewable energy with a large magnitude (630,000 EJ/yr on the land surface) [2], solar energy is increasingly becoming an appealing source of electricity worldwide [3, 4]. Photovoltaic cells are usually installed on rooftops to reduce reliance on the public electricity network [5]. In addition, semitransparent photovoltaic cells have provided an alternative substitute to conventional window glass [6, 7, 8, 9, 10], generating considerable amounts of electricity and allowing less solar radiation

*Corresponding author
Email address: ls.charles@polyu.edu.hk (Man Sing Wong)

to penetrate indoor spaces, thus eventually reducing energy needs for air conditioning. This benefit would be substantial for cities where air conditioners are intensively used over almost the entire year, such as Hong Kong and Singapore. Additionally, photovoltaic roads have been recently built [11, 12]. These applications imply excellent potential for utilizing solar energy in cities. Therefore, mapping the distribution of annual solar irradiations and understanding the effect of urban morphology on solar capacity is imperative for the systematic and practical use of solar energy.

In order to investigate the effect of urban morphology, it is vital to provide an accurate estimation of solar energy in an urban environment. Many studies estimated photovoltaic potential on rooftops [13, 14, 15, 16, 17], in which a study estimated solar photovoltaic potential on rooftops in Hong Kong by incorporating a cloud probability map [16]. Since cloud cover can determine solar energy on urban envelopes, possibly with seasonal variation, we will also use historical data on cloud cover to determine direct solar irradiation from the atmosphere.

Other studies in estimating solar energy mainly focused on façades associated with ground [18] or rooftops [19, 20, 21, 22]. For instance, one study proposed an algorithm to generate hyper points on façades so that each point enriches with solar irradiation [19]. In the same strategy, we will model a city as three-dimensional (3D) point clouds covering the whole urban envelopes to present annual solar irradiation on the clouds. The other two studies mainly contributed to the visualization of solar irradiation [21, 22], which incorporated a *r.sun* model and achieved real-time rendering by applying the technology on graphics processing unit acceleration. However, it has not considered a scenario that neighborhood buildings may interrupt solar irradiation significantly, which is non-negligible, particularly in megacities where skyscrapers clusters. Thus, overcoming this challenge becomes one of our research objectives. Another study emphasized the effect of greenery on receiving solar irradiation [23], which, however, will not be considered in our study because buildings are the most critical entity that fundamentally determines urban morphology in cities.

Further studies estimated solar irradiation on *all* three partitions, including rooftops, façades, and ground [23, 24, 26, 25, 27]. In particular, one study utilized the *r.sun* model to compute the segmentation between 3D vectors and the polygons and hence estimated shadows created by surrounding buildings [25]. Two similar studies examined whether a 3D vector intersects with a voxel to calculate solar irradiations on building surfaces [26, 27]. However, it is uncertain about applying these models to buildings with complex geometries. For example, two façades respectively belonging to two buildings may *touch* with each other so that the lower façade will never make shadows, footprints of buildings may be *concave* polygons so that shadows will project on itself, and the footprints may *nest* with each other that make irregular shadows. Since cities are likely having a variety of layouts and structures, and creating a reliable 3D solar city is crucial to investigate the urban morphology effect, addressing all these scenarios becomes crucial in our study. Our study will also make 3D intersections between *all* the radiation vectors and *all* the buildings containing different geometrics to construct shadows even made by far-away buildings, which thus can be applied for cities having a high density of tall buildings.

Different from rural areas, buildings are significant entities in urban areas that may equip with a large area of glass or mirrors with high albedo so that reflective radiation may alter the solar distribution significantly, making solar accumulation or dispersion in specific locations. A few studies indicated the capability of incorporating reflective radiations. For example, *r.sun* included the reflected component on horizontal or inclined surfaces [28, 29], SOLENE allowed a multi-reflection process in the indoor architecture space [30], Daysim computed irradiation accounting for all the light, direct and inter-reflected from the sky patch [31], and RADIANCE supported reflected radiation on buildings [32, 33, 34]. However, the method of managing accumulative and dispersive processes of the reflective radiation between urban envelopes is unclear, and it is uncertain for the capability of these

models to compute large urban areas with numerous buildings. The two deficiencies motivate us to propose a reflective module for estimating annual solar irradiation. It is vital because the albedo of urban envelopes is comparatively higher than in rural areas, and reflective radiation may constitute a considerable proportion of global radiation, especially in some locations with irradiation accumulation or dispersion.

A few studies investigated the relationship between urban morphology and solar irradiation in urban areas. Some explored relationships between urban geometry and solar accessibility in different temporal scales, which focused on rooftops and façades in several hours of a day [27], orientations of tilted roofs and façades subject to seasonality [35], and a wide range of building densities in different seasons [18]. In comparison, we will investigate the capacity of a city to maintain solar energy over an entire year, which is particularly important for practical implications such as the installation of photovoltaic cells. In another aspect, the effect of street characteristics on solar irradiation was explored. One proposed an indicator, which equals to the difference of the building heights divided by distance between buildings, to analysis its influence of solar radiation on façades [36], versus one investigated the relationship between different orientations of buildings and solar irradiation on tilted roofs and façades [35]. Instead of focusing on a single characteristic, the other two studies proposed several indices of urban morphology to explore their relationships between solar accessibility on building envelopes, and analyzed several scenarios of urban morphology and tested variables of urban form in order to increase solar energy potential for better urban design [37, 38]. Comparing with the above studies that either relied on a simulated urban form or a single city, our study aims to obtain a universal knowledge of the effect of urban morphology through analyzing the solar capacity of several cities globally.

In summary, our study will make a four-fold contribution. First, it models 3D shadows made by all buildings, which is particularly essential for urban areas with high-rise and high-density buildings. Second, our work incorporates *multiple* reflections with direct solar radiations between the urban envelopes with various types of geometries, which includes not only rooftops and the ground but also façades in a variety of orientations. Third, it allows fast computation of large amounts of buildings. Most importantly, we will reveal the effect of urban morphology on the solar capacity of 3D cities. The approach proposed herein also can be applied to urban heat island mitigation [39, 40], building daylight planning [27], and urban mobility [41, 42].

This paper is organized as follows. Section 2 defines the concept of solar capacity. Section 3 constructs a 3D solar city, which incorporates direct and diffuse irradiations from the atmosphere with *multiple* reflective irradiations between urban envelopes. Section 4 introduces data collection and validates the model. Section 5 explores the ability of ten cities across the world to utilize solar energy. Then, Section 6 investigates the distribution of quantitatively high and spatially concentrate solar irradiations in three partitions on rooftops, façades, and the ground. Furthermore, Section 7 investigates the effect of urban morphology on solar capacity through correlation analysis. Finally, Section 8 and Section 9 make a discussion and conclusion.

2. Definition of the solar capacity

Annual irradiation is defined as the solar irradiation that, starting from the incoming atmospheric irradiation, remains after the process of *multiple reflections* between urban envelopes. However, the confounding factor of different weather conditions for different cities may obstruct the detection of urban morphology on annual irradiations. For example, two cities with the exact same urban morphology and latitude would still have a big difference in total irradiations if one city is sunny while the other one is cloudy throughout a year. Thus, instead of investigating annual irradiations,

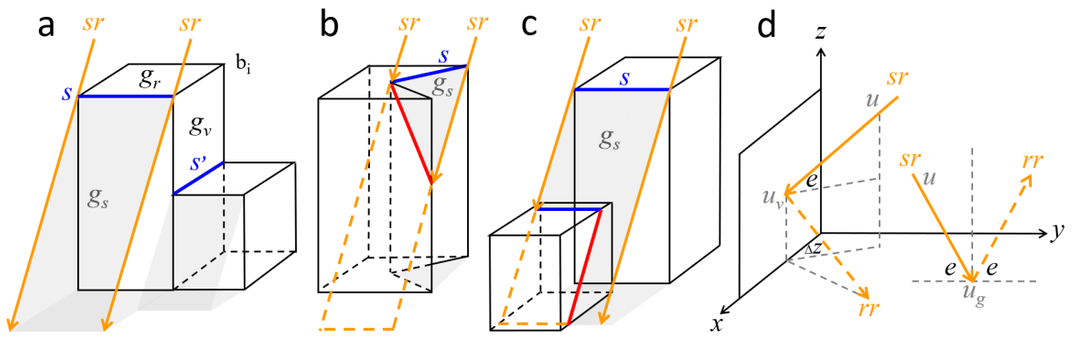

Figure 1: The method used in the multiple reflection model. (a) Solar radiation sr passing through s makes a 3D shadow polygon g_s, and s' will never make a shadow polygon. (b) When a rooftop is a concave polygon, g_s may intersect another façade of the same building as a red shadow line. (c) Shadow lines on façades and rooftops of other buildings will be used to make a correct g_s. (d) Irradiations on the façade (u_v) and ground (u_g) are derived from u.

the concept of solar capacity (cap) to describe the ability of different morphologies to utilize solar energy is proposed, which equals the total amount of annually maintained irradiation in an urban area (u_a) divided by the total amount of annual irradiation from the atmosphere in the same size of a flat area without any infrastructure (u), i.e., $cap = \frac{u_a}{u}$. According to the definition, the solar capacity is an appropriate index that allows us to focus on the capability of urban morphology to utilize solar energy. The notion of solar capacity is not influenced by specific weather conditions, as it is based on the transformation of annual irradiation to the *percentage* of the annual irradiation that remains after multiple reflections in a specific urban morphology.

3. Construction of a 3D solar city

A strategy for constructing a 3D solar city is presenting the urban envelopes (i.e., rooftops, façades, and ground) as 3D point clouds, and each point has a thematic attribute, e.g., the total solar irradiation accumulated over a year. At an instant of time, point clouds under sunshine or shadows can be simply determined by investigating intersections between 3D polygons of shadows and 3D polygons of urban envelopes. More specifically, point clouds on rooftops and ground are under shadows if they are below a 3D shadow polygon but inside the polygon in the orthographic projection. Similarly, point clouds on façades are also under shadows if they are orthographically below a 3D shadow line, i.e., the intersection between 3D shadow polygons and 3D façade polygons. Alternatively, point clouds are under sunshine if they are above the shadow polygons or shadow lines.

3.1. A city as 3D point clouds

In a 3D city, a building (b_i) has a rooftop (g_r) and a set of vertical façades ($g_v = \{g_1, ..., g_n\}$), all of which are recorded as 3D polygons. A rooftop g_r coincides with a façade g_x ($x \in [1, n]$) as a line segment s (Figure 1a). The ground (g_g) can be discretized as spatially contiguous and homogeneous grid cells with a resolution of d so that points can be generated at the center of the grids. Hence, 3D point clouds on g_r and g_g can be obtained and denoted by P_r^i and P_g, respectively. Similarly, g_v can be discretized as a set of vertical grid cells in the same d so that point clouds on g_v can be derived and represented as P_v^i, where their heights increase gradually from 0 to the height of buildings with a constant interval of d. Finally, point clouds on b_i can be organized as $\{P_r^i, P_v^i\}$ ($i \in [1, k]$), and a 3D city can be denoted by $\mathcal{P} = \{P_r, P_v, P_g\}$.

3.2. 3D shadow surfaces

Solar radiation that passes through the atmosphere from elevation e and azimuth z has solar irradiation u at an instant of time t and location l, i.e., $sr = \langle u, e, z, t, l \rangle$. A shadow polygon g_s

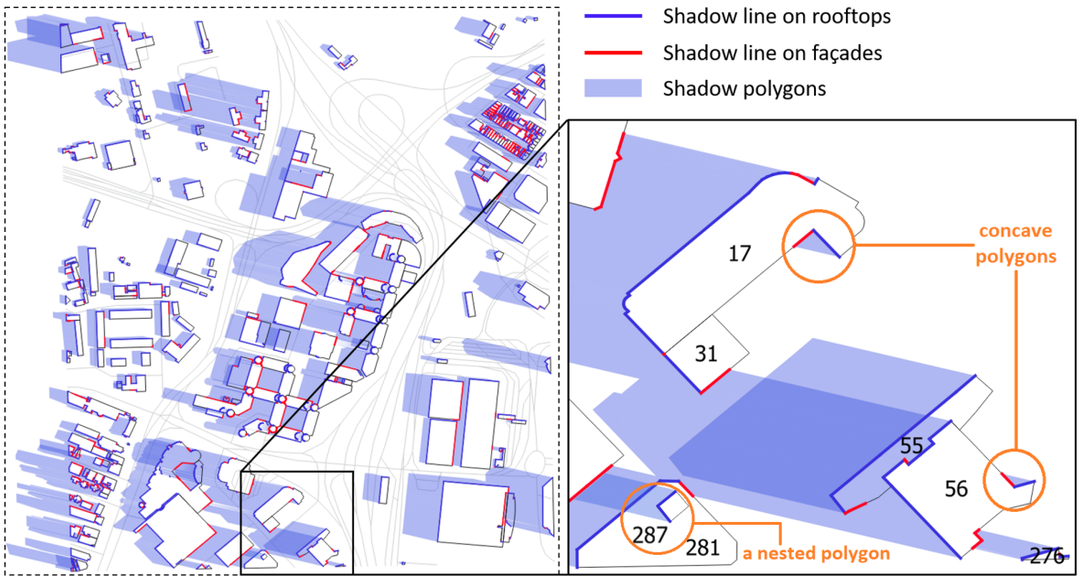

Figure 2: Shadows of buildings visualized in 2D. Each shadow is represented by a 3D polygon, where space below the polygon is in the shadow. Blue lines and red lines are intersection lines where 3D polygons intersect with the buildings on the façades and rooftops, respectively. Concave and nested polygons are also marked with the orange circles.

in parallel with sr will form when sr passes through the rooftop at the line segment s, which is a 3D parallelogram that divides sunshine from a shadow. The initial shadow polygon needs three modifications to make shadows physically correct. First, if two façades of two buildings *touch* with each other at a line segment s, then g_s belonging to the lower building will be removed since the lower façade will never make shadows (Figure 1a). Second, g_s may pass through several façades of the same building as a set of 3D shadow lines since the rooftop g_r is a *concave* polygon; however, this cannot happen in reality. In this case, the 3D shadow lines will generate a set of *false* shadow polygons that are unified as a single one g_p. Hence, g_p will be cut off from g_s, which means that g_s replaces $g_s = (g_s - g_p)$ (Figure 1b). Third, g_s created from a single building b_i may also be obstructed by façades and rooftops of the other building b_j. In more detail, g_s may pass through façades and/or rooftops of b_j as a set of 3D shadow lines that also generate *false* shadow polygons, which will be unified as $g_{p'}$. Thus, g_s will be modified as $g_s = (g_s - g_{p'})$ (Figure 1c). On top of this, physically reasonable shadows in the study area can be derived as $\mathcal{G} = \{g_s\}$, and all the 3D shadow lines are denoted by $\mathcal{S}$ (Figure 2).

3.3. Point clouds in sunshine and shadows

At this stage, 3D point clouds in $\mathcal{P}$ can be determined to be either in sunshine or in shadow. First of all, $\mathcal{G}$ and $\mathcal{S}$ are orthographically projected as $\mathcal{G}'$ and $\mathcal{S}'$, respectively. Point clouds in P_r and P_g are in shadow if their orthographic projections are located in $\mathcal{G}'$. Similarly, point clouds in P_v are in shadow if they are below a 3D shadow line in $\mathcal{S}$ and their orthographic projections, are on the corresponding shadow line of $\mathcal{S}'$ (Figure 3a). Based on a solar radiation sr, the solar irradiation of point clouds in the sunshine and on horizontal surfaces (i.e., rooftops and the ground) is computed as $u_r = u_g = u\sin(e)$ according to the energy conservation law. In contrast, the solar irradiation of point clouds in the sunshine and on vertical surfaces (i.e., façades) is computed as $u_v = u\cos(e)\sin(z^*)$, where z^* is the difference between the azimuth of the incoming radiation z and the azimuth of reflective radiation z' (Figure 1d and Figure 3b).

3.4. Multiple reflections of solar radiation

A point p ($p \in \mathcal{P}$) is assigned to solar irradiation larger than 0 means that p has already received direct solar radiation sr. The sr, having arrived at the exterior surface of the urban area, will reflect

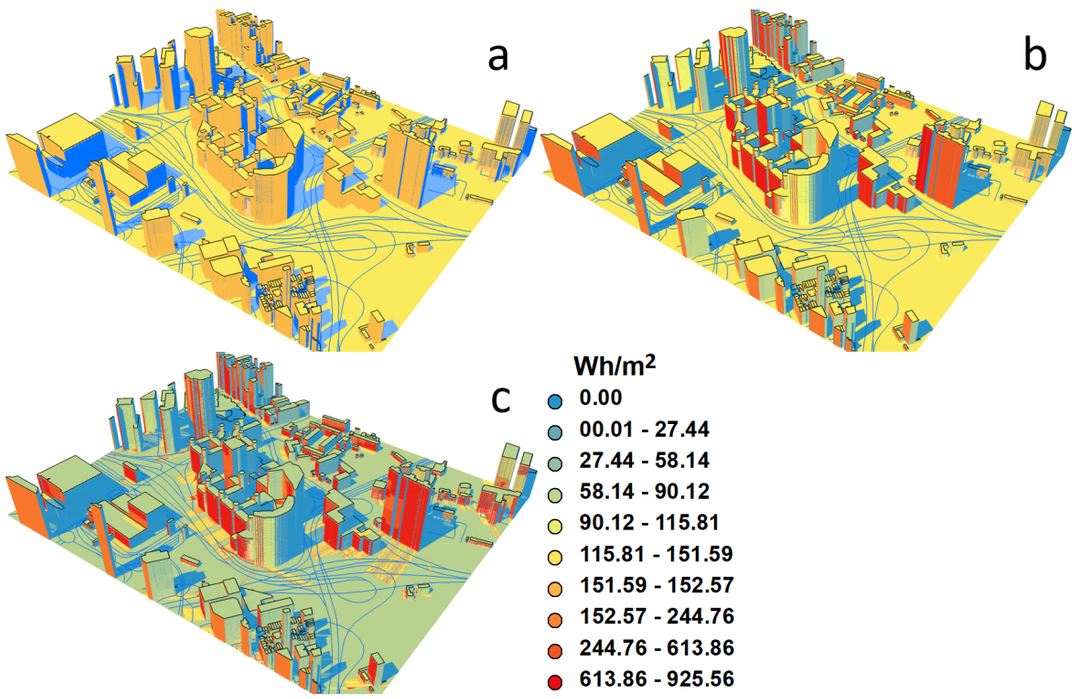

Figure 3: Visualization of 3D point clouds in HK in three continuous processes at an instant in time on a particular day. (a). 3D points in the shadow are visualized in blue, and 3D points in the direct solar radiation are visualized in yellow. (b). Direct incoming solar radiation irradiations at an instant of time on a particular day. (c). Solar irradiations with four iterative reflections. Some exterior urban surfaces accumulate less solar irradiations after the reflections because of the albedo, such that solar radiation towards the sky, taking away certain amount of the irradiation.

and become reflective radiation denoted as rr. More specifically, sr arriving at rooftops will reflect as rr and radiate upward with e and z unchanged. On the other hand, sr arriving at façades will also reflect as rr and further radiate downward with e unchanged while z is changed. When sr from the sky and rr from façades arrive at horizontal surfaces (i.e., rooftops or the ground), they will further transmit from the surfaces and directly radiate toward the sky or arrive at other façades with more reflections, and toward the sky ultimately (Figure 3c).

We assume that a complete set of direct solar radiation $R = \{sr\}$ has arrived at point clouds with solar irradiation larger than 0. Then, all the radiation in R may have multiple reflection processes, as presented previously, which will incorporate into an iterative computational framework. In each reflection, sr will contribute an amount of the irradiation to the associated point clouds and maintain the remaining amount as rr according to a determined albedo (δ). When sr arrives at a surface (either a rooftop, a façade, or the ground) and intersects the surface as a point o, a circular buffer centered at o with a radius of r is created on the surface and is represented as $\odot$. As a result, point clouds in $\odot$ are associated with sr, meaning that the irradiation will distribute to the point clouds evenly. Notably, during a reflection process, a point may receive a set of irradiations coming from different solar radiations, leading to an accumulation process.

4. Empirical investigation

4.1. Study area

To obtain a universal knowledge of the effect of urban morphology on the solar capacity, we selected ten cities across the world, which belong to several representative climates and were located at a range of 1.35° to 48.86° in latitude. Since some cities have distinctly different urban morphologies, two study areas were also selected carefully for comparisons in each city, which are the downtown area with dense and relatively taller buildings (abbreviations appended by h) versus the residential area with sparse and relatively lower buildings (abbreviations appended by l) (Table 1). For example, TOh and TOl represent a typical downtown area and a typical residential area in Toronto, respectively.

No.	Cities	Climate	Averagely tall (h)	Averagely low (l)
1	Athens	Mediterranean	ATh	ATl
2	Honolulu	semi-arid tropical	HOh	HOl
3	Hong Kong	subtropical	HK	-
4	Lisbon	Mediterranean	LBh	LBl
5	Los Angeles	dry subtropical	LAh	LAl
6	Mandalay	subtropical	-	MA
7	New York	humid continental	NY	-
8	Paris	continental	PAh	PAl
9	Singapore	tropical	SG	-
10	Toronto	continental	TOh	TOl

Table 1: Abbreviations of the study areas having averagely tall buildings verses averagely low buildings in ten cities.

4.2. Data collection

There is a challenge to obtain detailed building models covering all the large urban areas; alternatively, we assume that rooftops are all flat. Based on footprints of buildings that are recorded as two-dimensional polygons enriched with a height attribute, three-dimensional (3D), or more rigorously, 2.5D cities can be constructed. All study areas are reasonably flat, so the effect of terrain variation on the distribution of solar radiation can be ignored. The building models in Hong Kong were obtained from the Lands Department of Hong Kong. Building models of five cities were obtained online, which include Singapore [43], New York [44], Los Angeles [45], Honolulu [46], and Toronto [47]. The model in Mandalay only has information on building levels [48], so the heights of buildings were estimated by assuming that each level was 3 meters in height. High-resolution Digital Height Models (DHM) for Lisbon, Paris, and Athens were also obtained freely online [49], and the point clouds were constructed with the height information extracted from the DHM. Then, the average height was derived as the height of the building for points located in each building polygon derived from OpenStreetMap [50].

4.3. Computation

To obtain u from the sun at a specific t and l, the Points Solar Radiation toolbox in the ArcGIS 10.3 software was used [51], the outputs of which demonstrate solar irradiation on the horizontal surface. Since cloud cover is one of the most important factors that influence u, the diffuse proportions and transmissivity of the atmosphere (β_{dif}, β_{tra}) were determined to calculate u precisely, from monthly cloud cover data collected over three years between 2015 and 2017 from World Weather Online [52]. To obtain the corresponding (e, z) of solar radiation at (t, l), we also used an online tool named Sun Position [53].

Annual irradiations were computed based on the accumulation of hourly solar radiations over a year at a constant spatial resolution of 1 m, which created several millions of point clouds in each study area so that the computation could be extremely heavy. Therefore, the model was implemented in a relational spatial database management system (PostgreSQL 11) to achieve fast computation. Preliminary investigation suggested that more than 95% of the radiation ultimately reached the sky after four iterative reflections. Thus, four iterative computations were conducted in each study area (Figure 4).

4.4. Accuracy assessment

To explore the accuracy of the multiple reflection model, we conducted field observations in the urban area of Hung Hom, Kowloon district of Hong Kong, which is one of the most densely built-up

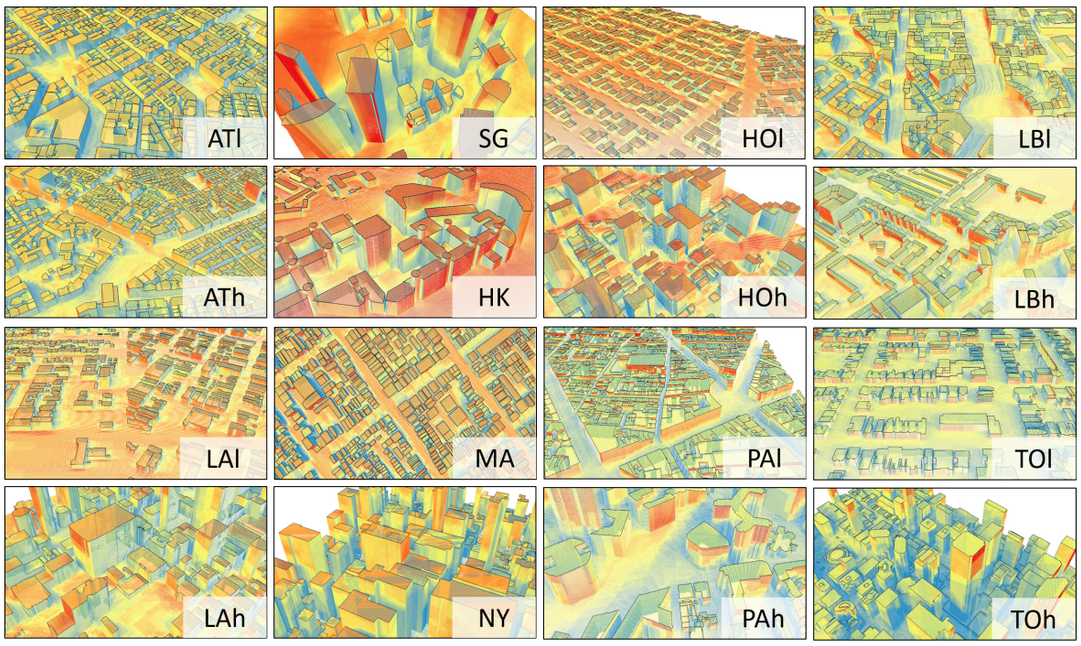

Figure 4: Annual irradiation, as resulting after the process of multiple reflections, in the 16 study areas of ten cities is visualized, with a detailed spatial scale of 500m×500m.

areas in the city. Seven valid observations were completed on bright sunshine days between January and May in 2018 to measure the photovoltaic potential. The area is the minimum bounding rectangle enclosing the sites with a 200 m outer buffer; thus, shadow and reflection effects caused by other buildings are therefore considered. The 3D building model was discretized as spatially contiguous and homogeneous grid cells at a 1 m resolution for both horizontal and vertical surfaces (Figure 5). The solar radiation meter captures almost all the global irradiation u_g coming from direct, diffuse, and reflective radiation at a specific t and l because the sensor is black, and the albedo is almost 0. However, the incoming solar irradiation u read from the profile is only contributed by direct and diffuse radiations. For removing this barrier, the estimated global irradiation expressed by u' can be computed as $u' = u + (u_n - u_1)$, where u_1 and u_n represent the irradiation derived from the first and n-th of the reflection, respectively. Then, relative errors between u_g and u' can be calculated. To determine a specific albedo (δ) used for systematic simulations, the albedos of common materials in cities are summarized (Table 2), and the average albedo is between 0.32 and 0.38. Based on this knowledge, each $\delta \in \{0.25, 0.30, 0.35, 0.40\}$ was used in the model for the case study in Hong Kong.

The results show that relative errors decrease significantly in almost all the estimations when considering reflections (Figure 6). As an exception, errors stay the same on the rooftops of Site 1 and Site 2 because the two rooftops have top heights in their surroundings so that no reflective radiation could contribute to the global irradiation. Specifically, the errors were lower than 0.1 in six observations out of nine when $\delta = 0.40$, which achieves a satisfactory accuracy for the estimations. Thus, the empirical evaluation indicates that the model can accurately estimate solar irradiations in both spatial and temporal domains. Additionally, $\delta = 0.40$ was used as an empirical parameter for the study.

5. Solar capacity of 3D cities

Annual irradiations in the ten cities were computed (Figure 7). The Pearson correlation coefficient between the cosine of latitudes ($cos(\alpha)$) and annual irradiations (u_a) is $R = 0.54$ and $p = 0.032$, which means that, as expected, a lower latitude tends to have larger annual irradiation. However, the correlation is only moderate, hinting at a possible role of urban morphology as a further determinant of

No.	Material	Albedo
1	wall brick	0.30
2	gypsum	0.35
3	ground asphalt	0.10 - 0.30
4	glasses (in average)	0.6895
5	concrete	0.17 - 0.27

Table 2: Albedos of materials commonly seen in cities [54, 55].

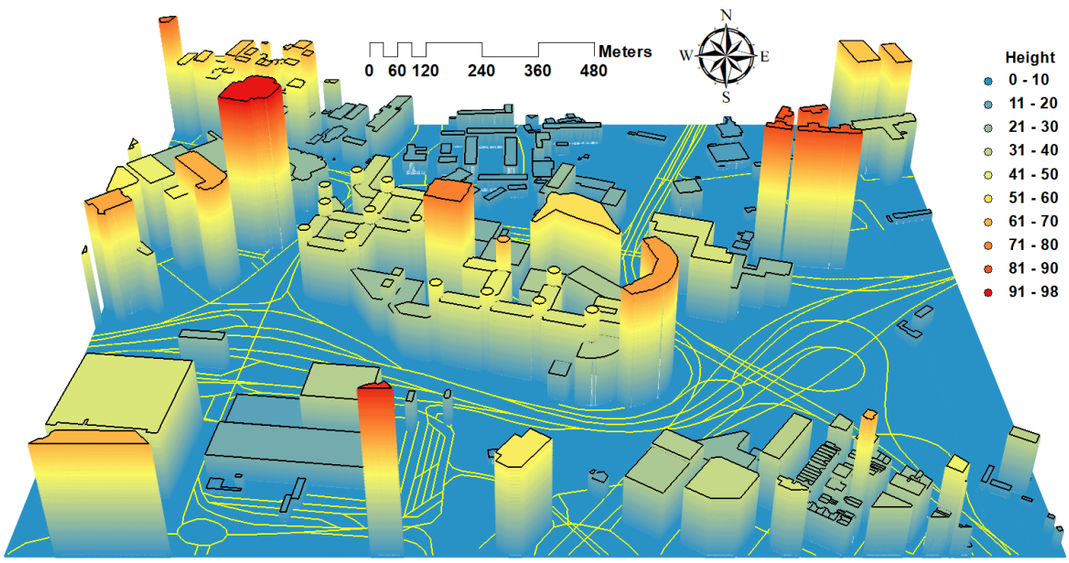

Figure 5: 3D point clouds of the field test sites. The area (945 m × 775 m) contains 302 buildings with heights ranging between 2 and 94 meters. Both horizontal and vertical resolutions of the 3D point clouds are 1m, which thus generates more than 1.4 million point clouds in total.

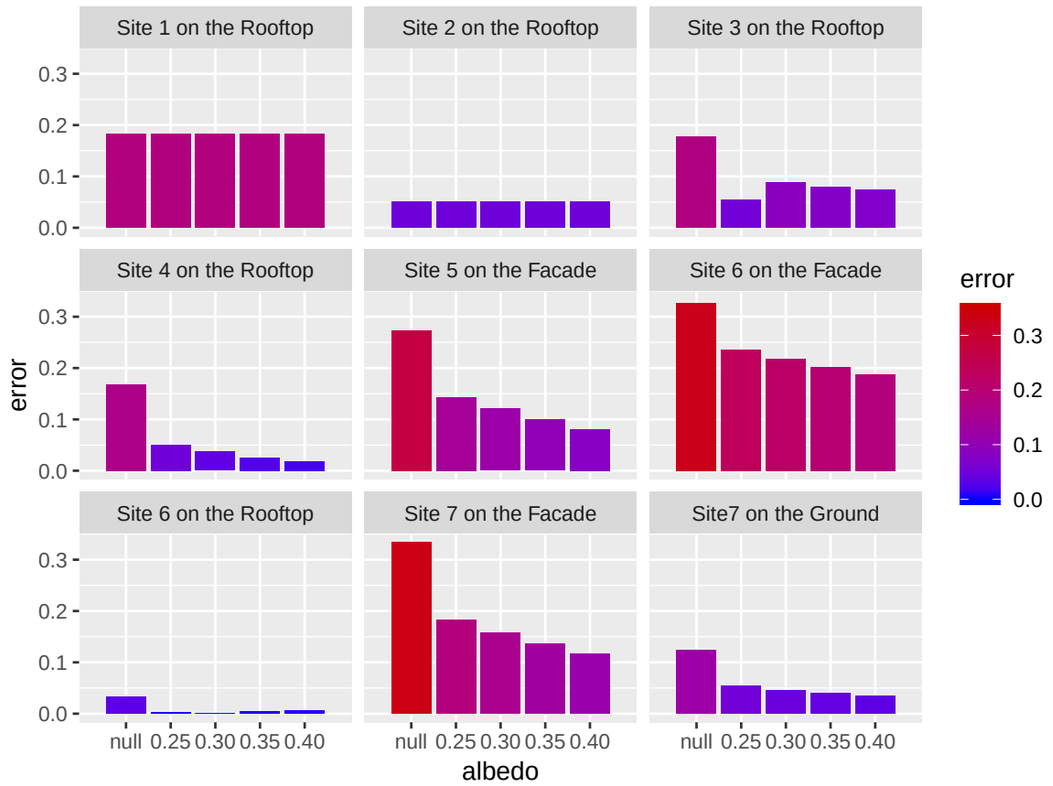

Figure 6: Relative errors between the observed and estimated solar irradiations lasting for six to seven hours over a daytime. The bars marked with *null* in the x-axis were derived from ArcGIS software without the functionality of multiple reflections; the remaining bars represent the estimations that account for reflections with different albedo values, ranging from 0.25 to 0.40. The seven sites include three types of location, i.e., rooftop, the ground, and façade.

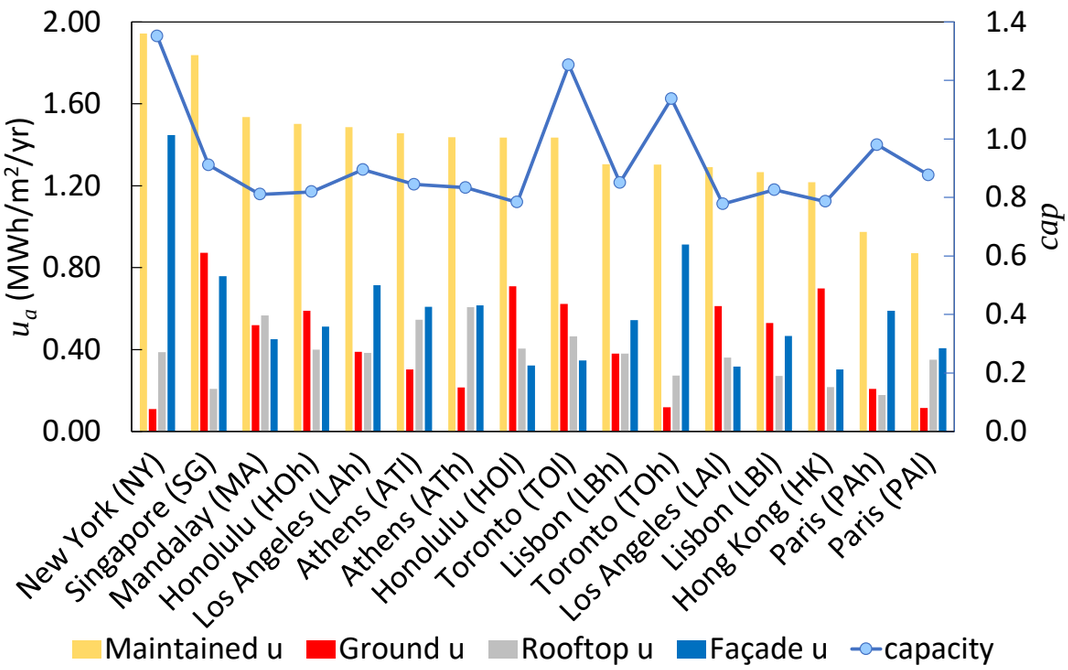

Figure 7: Annual irradiations in 16 the study areas of ten cities across the world. The yellow bar presents the total amount of irradiations maintained by urban surfaces together with their partition into ground, rooftop, and façade components. The blue line shows the solar capacities for the 16 study areas.

a city's solar capacity, an aspect that will be thoroughly analyzed in this study. Regarding correlations, areas with many high buildings can maintain larger irradiations, which becomes more noticeable when comparing two study areas in the same city and a significant exception occurs between TOh and TOl. Such a comparison also shows that SG ($\alpha = 1.35°$), MA ($\alpha = 21.96°$), and HOh ($\alpha = 21.30°$) have abundant u_a. However, u_a in HK ($\alpha = 22.39°$) is rather low even though it still has a low latitude. This is principal because HK is mountainous, with a humid subtropical climate and frequent cloud cover, which significantly reduces solar radiation. Since PAh and PAl have similar cloud covers as HK according to historical weather data, the lower u_a of PAh and PAl can be caused by a lower annual direct irradiation at the higher latitude, even though they have higher solar capacities. Notably, NY ($\alpha = 40.71°$), TOh, and TOl ($\alpha = 43.65°$) have remarkably high u_a even though their latitudes are above 40°. Their large solar capacities ($cap > 1$) indicate that they can maintain higher solar irradiations than over the same unit of flat area. This is probably because of the tall and dense buildings in the three areas, which is supported by clear evidence that façades in NY and TOh take a high proportion of the total irradiation.

A boxplot is presented to illustrate the numerical distributions of annual irradiations in ten cities (Figure 8). MA, HOl, SG, and LAl have considerably large irradiations since they have the largest irradiations at the third quartile with a wide range between the third quartile and the maximum. In the next four cities, ATl has the largest solar irradiation, followed by LBl, HOh, and HK with their third quartiles being almost the same. Study areas ATl, LBl, and HOh show higher probabilities than HK in utilizing large solar irradiations because the largest irradiation of HK is smaller than 1.50 MWh/m^2. In comparison, the third quartiles of LBh, ATh, LAh, and TOl decrease gradually while their maximums maintain large values approximately 2.00 MWh/m^2, which implies that their large irradiations may also be used efficiently. The last four cities of NY, PAl, PAh, and TOh have the smallest third quartiles, and their maximums are all smaller than 2.00 MWh/m^2, thus showing a weak probability of utilizing large irradiations. The figure also reveals two patterns. First, the ranking of cities according to the third quartile is very similar to the ranking of the latitude, even considering the effect of cloud cover. Second, study areas having low-average building heights always have a larger third quartile than high-average building heights in the same city.

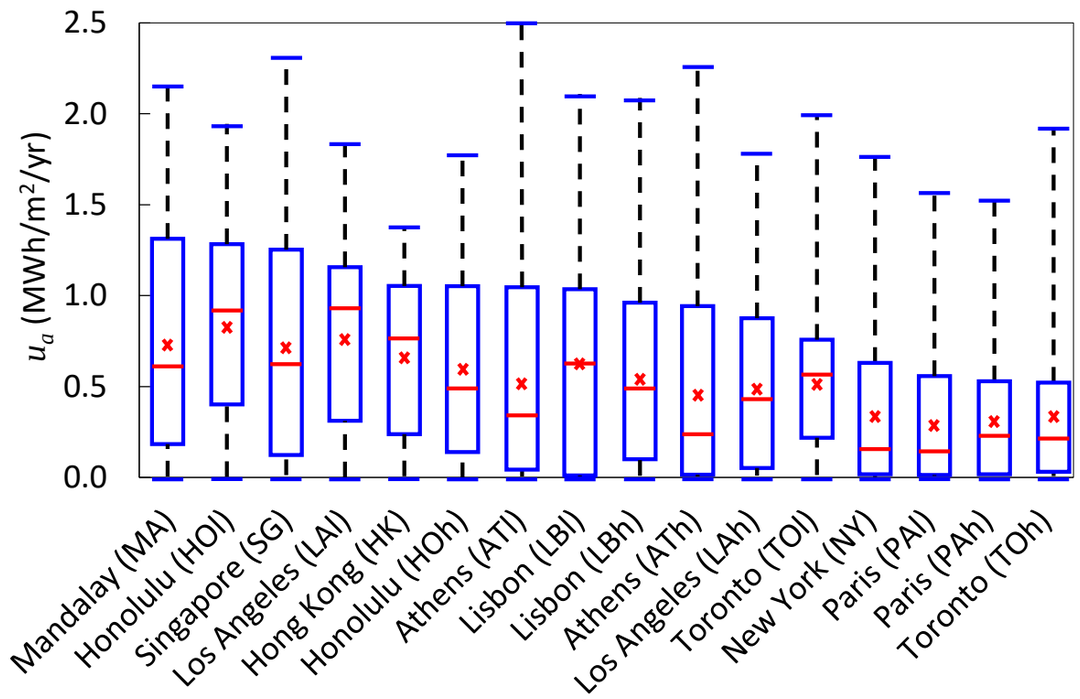

Figure 8: Distribution of the annual irradiations u_a of 3D point clouds for the ten cities. The y-axis reports the annual irradiations of point clouds in unit of MWh/m^2. On the x-axis, cities are ranked by annual solar irradiations at the third quartile.

6. Spatial distribution of solar irradiations

Solar irradiations that are both numerically high and spatially concentrated are always preferred for many purposes, such as installing photovoltaic cells in cities. The efficient use of solar irradiations is unlikely if the distribution of the irradiations is fragmented. To explicitly understand the usability of solar irradiations in urban areas, spatial clusters of the irradiations on demand have been investigated in three partitions. Overall, study areas with lower buildings can provide more ground area $p(a)$ of given street blocks $p(b)$ to satisfy the solar irradiation demand (Figure 9). For example, in HOl, at least 70% of the area ($p(a) = 0.7$) in 40% of the street blocks ($p(b) = 0.4$) can meet the criterion where solar irradiations are equal to or higher than 50% of the maximum irradiation u_m (Figure 9b). However, $p(a)$ is correspondingly only 0.4 in HOh. The figure also shows that HK and SG can maintain $p(a)$ effectively with the increase of the demand from $0.25u_m$, $0.50u_m$, to $0.75u_m$. This ability to maintain high values of $p(a)$ likely comes from their locations in low latitudes so that solar radiation at high elevations has a stronger ability to reach the ground. In contrast, $p(a)$ of the other cities drops off significantly when the demand increases. NY and ATh specifically have the lowest $p(a)$ for a given $p(b)$, since the densities of buildings in the two study areas are high and the elevations of solar radiation are small.

Similar to the ground, rooftops in study areas with lower average building heights have higher usability of solar irradiations if other factors remain constant (Figure 10). For instance, $p(a)$ in NY, SG, and HK is lower than in HOl and LAl at a given $p(r)$ (Figure 10b). This phenomenon becomes even more apparent for two study areas in the same city, such as HOl versus HOh (Figure 10b) and TOl versus TOh (Figure 10e). Additionally, with the increase of $p(r)$ when the demand equals to $0.25u_m$ and $0.50u_m$, most curves in Figure 10 decrease dramatically initially and then have a long and slight decrease followed by another dramatic decrease at the end. This indicates that large solar irradiations can be utilized on most rooftops, but the usable areas of large irradiations in these rooftops are limited. Besides, a small proportion of the area $p(a)$ can still utilize the highest demand of solar irradiations in SG, HOh, and HK in a small proportion of rooftops $p(r)$ (Figure 10c). These rooftops are expected to be on high-rise buildings so that they are not affected by shadows most of the time.

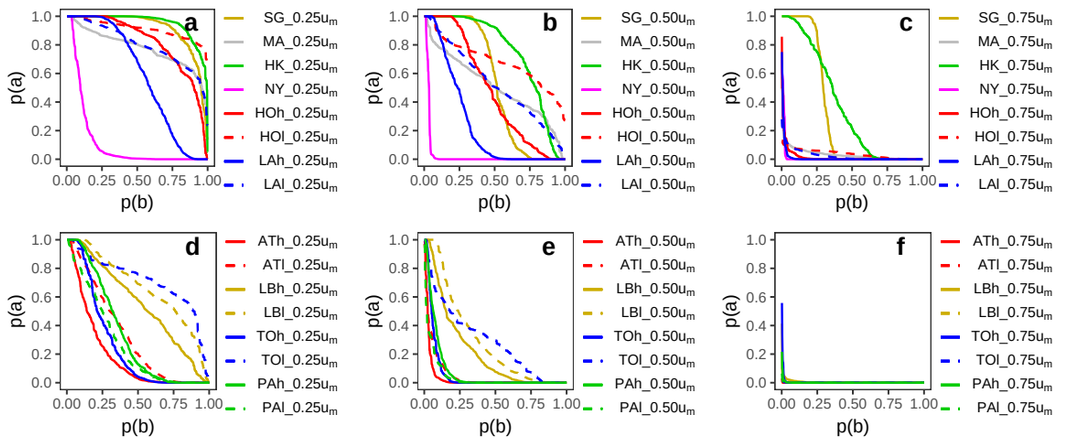

Figure 9: Spatial clustering of the demand solar irradiation on the ground. At least $p(a)$ proportion of the area (y-axis) in $p(b)$ proportion of the street blocks (x-axis) has solar irradiations equal or larger than $(100x)\%$ ($x = \{0.25, 0.50, 0.75\}$) of the maximum irradiation (u_m) on the ground. Specifically, street blocks are spatial contiguous and homogeneous grid cells in resolution of 50m. For two study areas in the same city, u_m equals to the larger value of the two maximums on the ground for fair comparison.

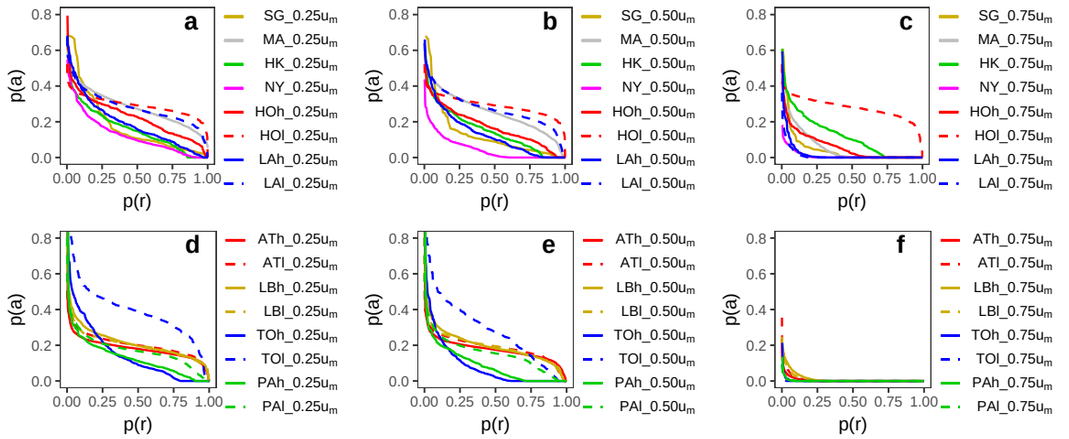

Figure 10: Spatial clustering of the demand solar irradiation on rooftops. At least $p(a)$ proportion of the area (y-axis) in $p(r)$ proportion of the rooftops (x-axis) has solar irradiations equal or larger than $(100x)\%$ ($x = \{0.25, 0.50, 0.75\}$) of the maximum irradiation (u_m) on the rooftop. For two study areas in the same city, u_m equals to the larger value of the two maximums on the rooftop for fair comparison.

Specifically, almost all the rooftops in HOl allow 20% of the area to utilize the highest demand at $0.75u_m$, since HOl is an area with low and sparse buildings, and solar radiation would thus easily arrive at most of the rooftops year-round.

In addition to the ground and rooftops, significant proportions of the area of some façades can be utilized effectively. More specifically, $p(a)$ can be maintained at 1.0 in most of the curves followed by a sharp decrease to the bottom with the increase of $p(v)$ (Figure 11), which means that façades can usually allow either maximum or minimum usability. This phenomenon is evident for study areas such as NY and HK, which have high-rise buildings on average, even with demand reaching up to $0.75u_m$ (Figure 11c). Other study areas in the same city follow the same pattern and do not have distinct differences except for HOh and HOl (Figure 11b and Figure 11e). The sharply decreasing trend without gradual changes is probably due to the orientations of façades, so façades with direct solar radiation can obtain maximum irradiations while façades continuously in shadow cannot obtain sufficient solar radiation even though multiple reflections of solar radiation may still contribute, such as in NY and HK.

All spaces including rooftops and the ground are scarce in urban areas, and utilizing façades of buildings to collect solar irradiations may be an effective strategy. Thus, a detailed investigation has been made of façades in the height domain. Overall, the average irradiation $v(u)$ increases while the

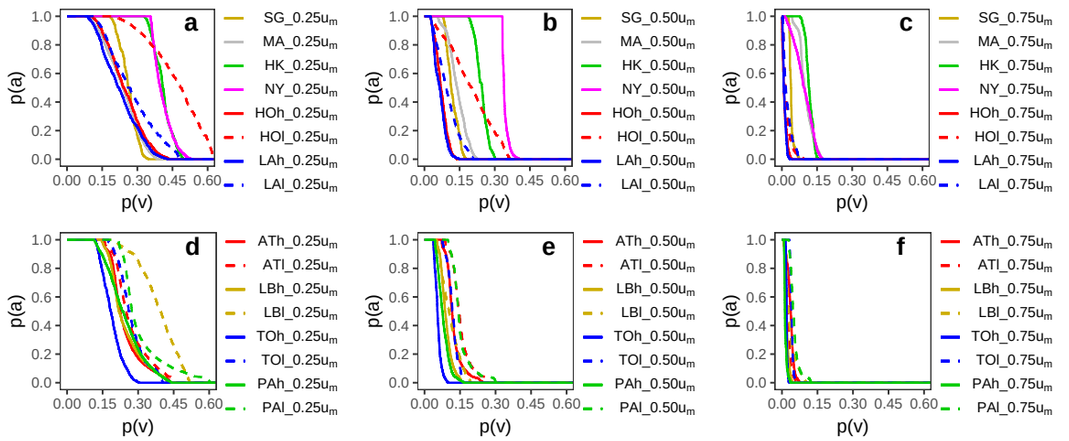

Figure 11: Spatial clustering of the demand solar irradiation on façades. At least $p(a)$ proportion of the area (y-axis) in $p(v)$ proportion of the façades (x-axis) has solar irradiations equal or larger than $(100x)\%$ ($x = \{0.25, 0.50, 0.75\}$) of the maximum irradiation (u_m) on the façade. For two study areas in the same city, u_m equals to the larger value of the two maximums on the façade for fair comparison.

proportion of the total irradiation $p(u)$ decreases gradually with the increase in the relative height $p(h)$ for all 16 study areas (Figure 12). The optimal location to utilize solar energy is the height at which large solar irradiations of individual point clouds meet large amounts of the total irradiation. For example, $p(h) = 0.5$ may be an optimal height for PAl where $p(u)$ reaches the peak and $v(u)$ is relatively high. Notably, some of the blue curves have a slight decrease, which makes a *saddle* shape when it approaches the largest height. This unique pattern occurs in many study areas such as LAl, ATl, NY, and PAl. In NY for example, $v(u)$ continuously meets the first inflection point when $p(h) = 0.5$, a *saddle* point at $p(h) = 0.6$, and the second inflection point when $p(h) = 0.7$. This may be because several buildings have already reached their largest heights when $p(h) = 0.5$, causing several large irradiations to make a large $v(u)$. A deficiency in the number of buildings occurs and irradiations decreases when $p(h) > 0.5$, leading to a decrease in $v(u)$ until $p(h) = 0.6$. Furthermore, irradiations become larger when the remaining buildings still exist with an increase of $p(h) \in (0.6, 0.7]$. Additionally, some of the red curves have conspicuous irradiation accumulations at near-ground façades. Taking again NY for illustration, irradiations concentrating at $p(u) = 0.1$ may have two reasons for their existence. First, large areas at $p(u) = 0.1$ have already obtained considerable amounts of the total irradiation from direct solar radiation. Second, reflected radiation from the ground and other façades provides further contributions that make $p(u)$ higher than in an area with smaller $p(h)$. This can also be seen intuitively by 3D visualizations of point clouds (Figure 4).

Next, we look at the azimuthal domain and investigate the influence of building orientation on the distribution of irradiations on façades. The analysis demonstrates that the distribution of the irradiation varies when aggregating the total solar irradiation on façades in eight directions (Figure 13). For example, solar irradiation in NY has even distributions from three directions, SE, SW, and NW, while it is insignificant from NE and is nearly zero for S and W. This coincides with orientations of buildings given that buildings in the NY study area are regularly oriented in a south direction. A similar phenomenon occurs in several other study areas, such as MA, TOh, and TOl. However, building orientations are inhomogeneous in study areas such as LBh and LBl, meaning the distribution occurs in almost all directions. Therefore, orientations of buildings can significantly affect the directional distributions of solar irradiations.

7. Effects of urban morphology

This principle, and the previously made observation about the moderate correlation of latitude with the annual irradiation, motivates our investigation of how urban morphology affects solar energy

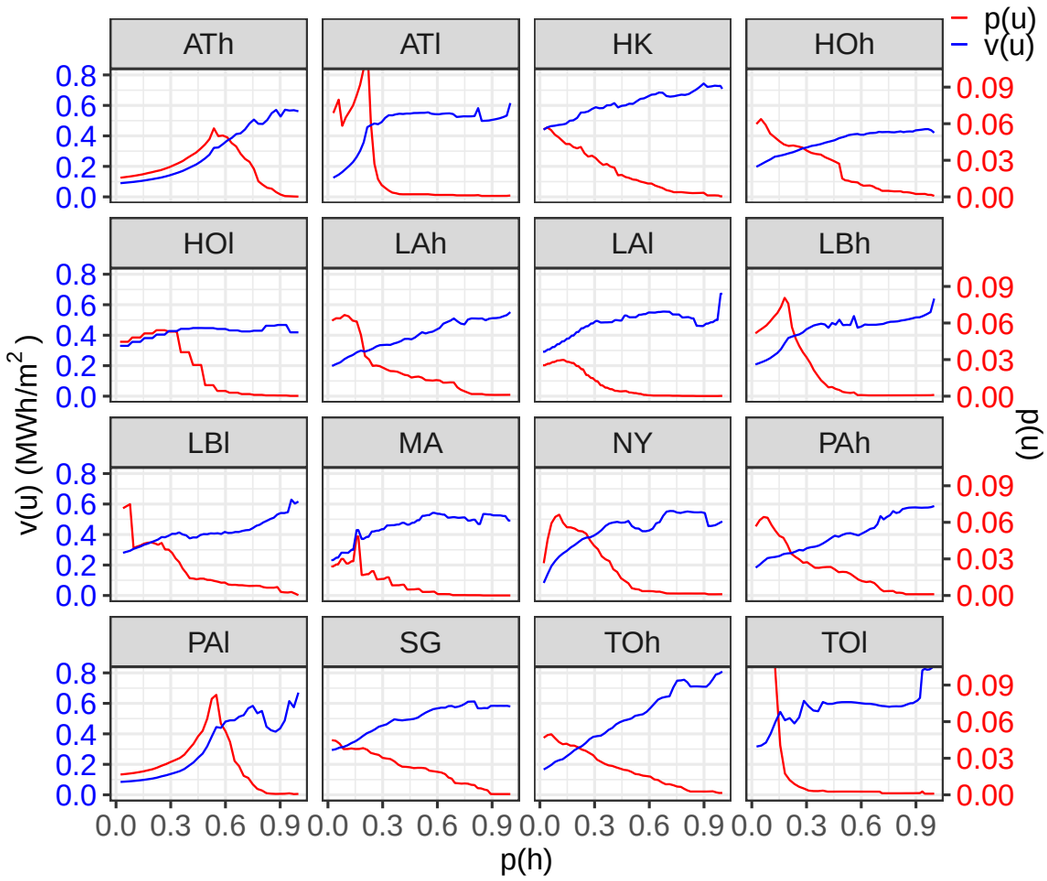

Figure 12: Distribution of solar irradiations along heights of façades. The average irradiation $v(u)$ is the blue curve and corresponds to the left y-axis. Proportion of the total irradiation $p(u)$ is the red curve and corresponds to the right y-axis, both of which are against heights of point clouds on façades relative to the maximum height denoted by $p(h)$ in the x-axis.

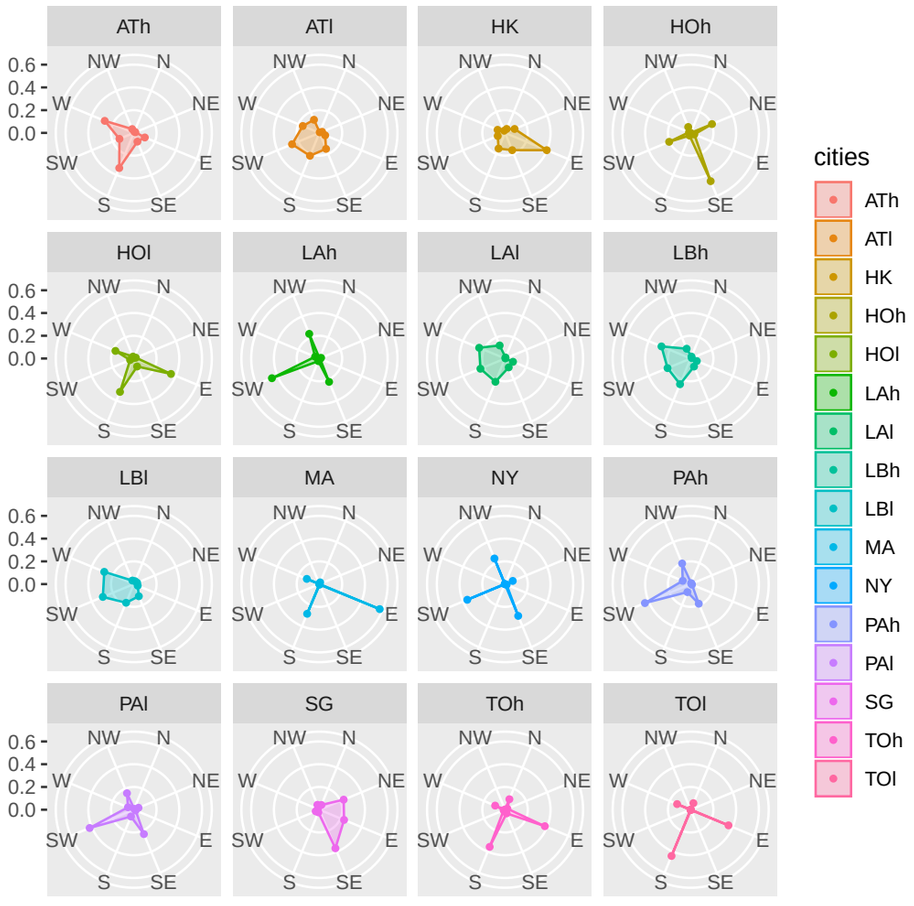

Figure 13: Distribution of proportion of the total irradiation on façades in eight directions.

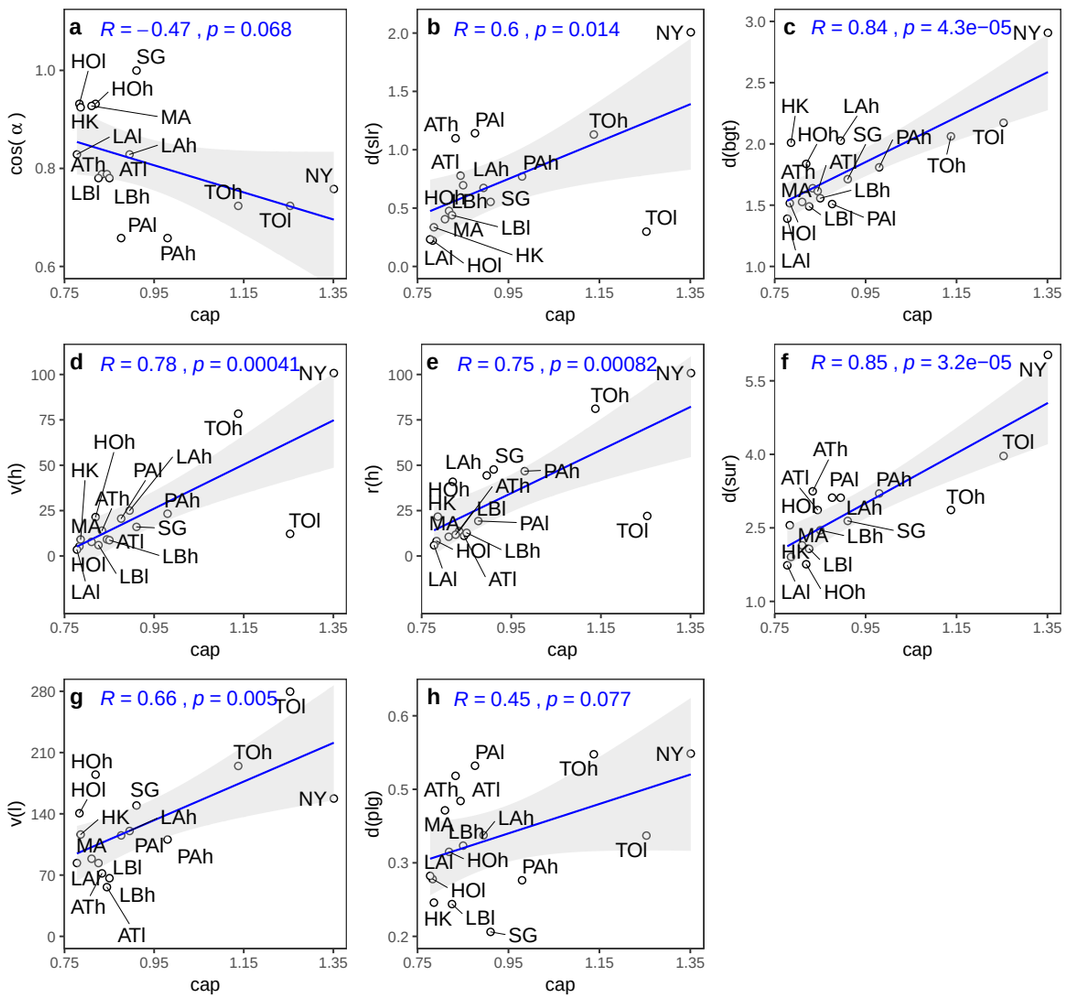

Figure 14: Pearson correlation coefficient (R) between eight indices and solar capacity. Solar capacity is on the x-axis, and eight indices on the y-axis from Figure 14a to Figure 14h are cos of latitudes $\cos(\alpha)$, the density of solar-face area $d(slr)$, the density of brightness area $d(bgt)$, the average height of point clouds in horizontal surfaces $v(h)$, the roughness of point clouds in horizontal surfaces $r(h)$, the density of exterior surface area $d(sur)$, the average perimeter of all the footprints of buildings $v(p)$, and the density of footprint areas $d(plg)$, respectively.

potential, and what urban morphology is most desirable to effectively utilize solar energy. Eight indices have been proposed to describe different aspects of urban morphology and then correlate with the solar capacity (Figure 14). Compared with u_a and $cos(\alpha)$, which have a positive correlation with $(R = 0.54, p = 0.032)$ as mentioned in Section 5, cap and $cos(\alpha)$ have obtained moderately negative correlations given $R = -0.47$, thereby suggesting that latitudes have a significant but not conclusive impact on solar capacity (Figure 14a). This reveals that cities at higher latitudes tend to have a relatively larger cap even though their u_a is generally smaller. A possible explanation for this result is that a higher latitude means a lower annual elevation of solar radiation, creating more reflections between façades, and leading to a relatively higher accumulation of irradiations.

Orientations of buildings may influence the solar capacity because statistics have suggested that solar irradiations on façades are different in different study areas (Figure 13). Therefore, the correlation between cap and the density of a solar-face area $d(slr)$ has been calculated as follows: $d(slr) = \frac{\sum(cos(d_i)a_i)}{sa}$ $(|d_i| < \frac{\pi}{2})$, where d_i is the azimuthal difference of each façade subject to the maximum annual azimuth of solar radiations, $|d_i| < \frac{\pi}{2}$ ensures that each façade is facing the incoming solar radiation, a_i is the area of the corresponding façade, and sa is the area of the study area. The analysis shows that cap and $d(slr)$ have a somewhat strong and positive correlation with $R = 0.60$ (Figure 14b), which means that the orientation of buildings can significantly influence the solar capacity of cities. Surprisingly, TOh has a smaller cap but a much larger $d(slr)$ compared with TOl, presenting a

negative correlation for the two study areas in the same city. Visualizing all the irradiations in 3D point clouds indicates that many high-rise buildings are located in the south and east part of TOh; therefore, a large amount of incoming solar radiation arrives at the buildings, and then reflects to the sky immediately, while the majority of buildings in the north and western parts are under the shadow, which results in lower irradiations being maintained by the buildings. Thus, *cap* decreases for TOh even though $d(slr)$ is larger. The two findings clearly illustrate the importance of orientational planning of buildings and associated locational height control to maximize the solar capacity.

Even when the façades in $d(slr)$ satisfy the condition $|d_i| < \frac{\pi}{2}$, some can still be blocked by other buildings and are essentially in shadow, such as in TOh. Therefore, the density of brightness areas, denoted by $d(bgt)$, was considered while disregarding the orientation of buildings. $d(bgt) = \frac{\sum(a_{bgt})}{sa} \mid (u_{bgt} \geqslant xu_m)$, which means that the total area of point clouds in brightness areas is divided by the entire study area, where the point clouds equal to or higher than x proportion of the maximum annual irradiation are viewed as the annual brightness area. Since boundaries between shadows and brightness are ambiguous in many urban areas, a set of values of x should be tested empirically to determine the brightness points. Interestingly, *cap* and $d(bgt)$ are in a very strong and positive correlation of $R = 0.84$ when $x = 0.1$ (Figure 14c). The analysis clearly shows that a larger $d(bgt)$ leads to a larger *cap* for any two study areas in the same city without any exception. The analysis also finds that some irradiation accumulations are not located in the solar-face area, thereby suggesting a significant contribution of multiple reflections from other buildings. Therefore, $d(bgt)$ appears more significant than $d(slr)$ in determining solar capacity.

One of the most apparent differences between study areas is the majority of high buildings in some cities versus a majority of low buildings in others, which creates distinct differences in urban morphology and may have certain effects on solar capacity. Therefore, the heights of all point clouds on horizontal surfaces of rooftops and ground, denoted by h, were investigated. The *cap* and the average height of the points $v(h)$ showed a somewhat strong and positive correlation of $R = 0.78$ (Figure 14d), meaning that a study area with overwhelmingly high buildings tends to have a relatively larger solar capacity. This may be mainly because high buildings can maintain large amounts of irradiation on façades (Figure 11). However, study areas with the same $v(h)$ may still have different solar capacities since the difference between each height and $v(h)$ can be different. Thus, the concept of the *roughness* of exterior urban surfaces is introduced to describe the topographic relief in study areas, which equals the standard deviation of the heights of the points in horizontal surfaces, and is represented by $r(h)$. The analysis shows that *cap* and $r(h)$ also obtained a somewhat strong and positive correlation of $R = 0.75$ (Figure 14e), which means that large erratic fluctuations in topography would lead to a large solar capacity. This is because the heights of buildings varying randomly allow solar radiation to pass through various parts of the urban area so that large amounts of irradiations can be maintained and accumulated through multiple reflections between buildings. For example, given two equal areas in the same location and having the same building footprints, one has the same height for all buildings and $r(h) = 0$, while the other has various heights of the buildings and $r(h) > 0$. All the radiation arriving at the rooftops will reflect toward the sky without any further accumulation of irradiations when $r(h) = 0$. In contrast, when $r(h) > 0$ radiation arriving at rooftops and/or façades can reflect onto façades and/or the ground with the accumulation of irradiations simultaneously.

Large areas of exterior urban surfaces, including ground, rooftops, and façades, will likely receive and maintain solar radiation. Motivated by this observation, the density of exterior urban surfaces was computed and denoted as $d(sur)$, which equals the total area of exterior urban surfaces divided by the flat area on which they locate. Surprisingly, *cap* has a very strong and positive correlation with $d(sur)$ of $R = 0.85$ (Figure 14f), which demonstrates that a large area of exterior urban surfaces can promote the maintenance of irradiations from direct and reflected radiation. Notably, $d(sur)$ is

determined by the area of façades since the total area of the ground and rooftops is deterministic and is equal to the flat area where it locates. Furthermore, the decomposition of the façade areas can be indicated by $v(h)$ (Figure 14d) and $v(p)$, which represents the average perimeter of all the footprints of buildings. Since *cap* and $v(p)$ have also obtained a somewhat strong and positive correlation of $R = 0.66$ (Figure 14g), this suggests that the correlation of $R = 0.85$ between *cap* and $d(sur)$ can be explained by the combined effect of $v(h)$ and $v(p)$. However, *cap* and $d(plg)$, which represents the density of all the footprint areas, only shows a moderately positive correlation of $R = 0.45$ (Figure 14h). This means that a large $d(plg)$ can lead to a large *cap*. Notably, study areas such as PAl, ATh, and ATl have a relatively high $d(plg)$ but a small *cap*. The reason for this result is that $d(plg) \geqslant 0.47$ calculated for the three study areas indicates that there is not much space between buildings. Hence, only a small proportion of the solar radiation can arrive at the top of façades, and most of the solar radiation reflects to the sky immediately after it arrives at the rooftops and on the ground. This phenomenon becomes even more evident for the three study areas since the heights of these buildings are rather homogeneous, i.e., $r(h)$ is small.

8. Discussion

The model supports rooftops in different geometrical shapes, e.g., a rooftop made by two slanting polygons, while the study assumes that all rooftops are flat due to lacking a high level-of-detail dataset. Nevertheless, this hypothesis should not cause a notably adverse effect because a vast majority of reflective radiations from the rooftops approach the sky immediately that will not make an influence on estimating solar irradiation on urban envelopes. Even though the albedo used in the study is a constant value derived from an empirical investigation, it will not make any effect on solar capacity and the correlation analysis with urban morphology because solar capacity is a relative index essentially that counts the percentage of the annual irradiation. More accurate albedo for each city can obtain from recognizing building materials that come from street-view images, and machine learning could be an effective way to process large amounts of the images. The model can also be improved to account for the influence of terrain variation and vegetation, which in some urban areas is highly relevant.

The specular reflection rule is used to approximate all the reflections to control the computational cost. Even a small area may contain millions of point clouds, so the intersections between all the reflective radiations and all the urban envelopes would generate thousands of millions of associations as an intermediate result, which would further burden an already cumbersome computation process. Thus, the diffuse reflection on concrete surfaces of the urban envelopes is simplified to maintain reasonable computational efficiency.

Having studied the structure of 3D solar cities, we can determine the optimal locations for utilizing solar energy based on each area's specific needs. For instance, installations of photovoltaic cells should be at locations where irradiations are both quantitatively high and spatially concentrated, vegetation for greenery purposes shall be in moderate sunshine, and thermal comfort routing planned for pedestrians should be under shadows.

9. Conclusion

This study proposed a solution to construct a 3D solar city, which considers not only direct and diffuse radiation from the atmosphere but also incorporates *reflective* radiation between 3D urban envelopes. The reflective module approximates solar distribution more accurately in an urban environment since high albedo in cities may alter the distribution significantly. Even though latitude and clouds influence total solar irradiation, urban morphology has a substantial impact on solar capacity, which thus makes a disruptive change on annual irradiation ultimately. It suggests that, in the same

condition (latitude and clouds), a city tends to have a larger solar capacity when it has a higher density of tall buildings and an erratic fluctuation of the building heights. The proposed indices of urban morphology can support local governments in strategizing urban development, and the robust computational framework of the model can be applied to provide adequate decision-making support for initiatives.

Acknowledgment

This work was supported in part by the grant from the Hong Kong Polytechnic University of a project "Potential of solar power development of PolyU campus using 3D building model", and National Research Foundation Singapore. The authors thank the Hong Kong Lands Department for the 3D building data provided.

References

[1] Chu S, Majumdar A. Opportunities and challenges for a sustainable energy future. Nature 2012; 488:294–303.

[2] Nakicenovic N, Gomez-Echeverri L, Johansson TB, Patwardhan A. Global Energy Assessment - Toward a Sustainable Future. Cambridge University Press; 2012.

[3] Ma S, Goldstein M, Pitman AJ, Haghdadi N, MacGill I. Pricing the urban cooling benefits of solar panel deployment in Sydney, Australia. Scientific Reports 2017; 7:43938.

[4] Molina A, Falvey M, Rondanelli R. A solar radiation database for Chile. Scientific Reports 2017; 7:14823.

[5] Fares RL, Webber ME. The impacts of storing solar energy in the home to reduce reliance on the utility. Nature Energy 2017; 2:17001.

[6] Fu F, Feurer T, Jaĝer T, Avancini E, Bissig B, Yoon S, Buecheler S, Tiwari AN. Low-temperature-processed efficient semi-transparent planar perovskite solar cells for bifacial and tandem applications. Nature Communications 2015; 6:8932.

[7] Vasiliev M, Alghamedi R, Nur-E-Alam M, Alameh K. Photonic microstructures for energy-generating clear glass and net-zero energy buildings. Scientific Reports 2016; 6:31831.

[8] Wheeler LM, Moore DT, Ihly R, Stanton NJ, Miller EM, Tenent RC, Blackburn JL, Neale NR. Switchable photovoltaic windows enabled by reversible photothermal complex dissociation from methylammonium lead iodide. Nature Communications 2017; 18:1722.

[9] Davy NC, Sezen-Edmonds M, Gao J, Lin X, Liu A, Yao N, Kahn A, Loo YL. Pairing of near-ultraviolet solar cells with electrochromic windows for smart management of the solar spectrum. Nature Energy 2017; 2:17104.

[10] Traverse CJ, Pandey R, Barr MC, Lunt RR. Emergence of highly transparent photovoltaics for distributed applications. Nature Energy 2017; 2:849–860.

[11] Golson, J. World's first 'solar panel road' opens in France, https://www.theverge.com/2016/12/22/14055756/solar-panel-road-electricity-france-normandy; 2019 [accessed 19 July 2018).

[12] GCR Staff. China set to win race for first solar expressway, http://www.globalconstructionreview.com/news/china-set-win-race-first-solar-expressway/; 2019 [accessed 19 July 2018].

[13] Izquierdo S, Montañés C, Dopazo C, Fueyo N. Roof-top solar energy potential under performance-based building energy codes: The case of Spain. Solar Energy 2011; 85:208–213.

[14] Jakubiec JA, Reinhart CF. A method for predicting city-wide electricity gains from photovoltaic panels based on LiDAR and GIS data combined with hourly Daysim simulations. Solar Energy 2013; 93:127–143.

[15] Li Y, Ding D, Liu C, Wang C. A pixel-based approach to estimation of solar energy potential on building roofs. Energy and Buildings 2016; 129:563–573.

[16] Wong MS, Zhu R, Liu Z, Lu L, Peng J, Tang Z, Lo CH, Chan WK. Estimation of Hong Kong's solar energy potential using GIS and remote sensing technologies. Renewable Energy 2016; 99:325–335.

[17] Calcabrini A, Ziar H, Isabella O, Zeman M. A simplified skyline-based method for estimating the annual solar energy potential in urban environments. Nature Energy 2019; 4:2058–7546.

[18] Chatzipoulka C, Compagnon R, Nikolopoulou M. Urban geometry and solar availability on facades and ground of real urban forms: using London as a case study. Solar Energy 2016; 138:53–66.

[19] Catita C, Redweik P, Pereira J, Brito MC. Extending solar potential analysis in buildings to vertical facades. Computers & Geosciences 2014; 66:1–12.

[20] Redweik P, Catita C, Brito M. Solar energy potential on roofs and facades in an urban landscape. Solar Energy 2013; 97:332–341.

[21] Liang J, Gong J, Li W, Ibrahim AN. A visualization-oriented 3D method for efficient computation of urban solar radiation based on 3D–2D surface mapping. International Journal of Geographical Information Science 2014; 28:780–798.

[22] Liang J, Gong J, Zhou J, Ibrahim AN, Li M. An open-source 3D solar radiation model integrated with a 3D Geographic Information System. Environmental Modelling & Software 2015; 64:94–101.

[23] Lindberg F, Jonsson P, Honjo T, Wästberg D. Solar energy on building envelopes – 3D modelling in a 2D environment. Solar Energy 2015; 115:369–378.

[24] Lobaccaro, G., Carlucci, S., Croce, S., Paparella, R. & Finocchiaro, L. (2017). Boosting solar accessibility and potential of urban districts in the Nordic climate: A case study in Trondheim. *Solar Energy*, 149, 347–369.

[25] Hofierka, J. & Zlocha, M. (2012). A new 3-D solar radiation model for 3-D city models. *Transactions in GIS*, 16(5), 681–690.

[26] Erdélyi, R., Wang, Y., Guo, W., Hanna, E. & Colantuono, G. (2014). Three-dimensional SOlar RAdiation Model (SORAM) and its application to 3-D urban planning. *Solar Energy*, 101, 63–73.

[27] Zhu R, You L, Santi P, Wong MS, Ratti C. Solar accessibility in developing cities: A case study in Kowloon East, Hong Kong 2019; 51:101738.

[28] Šúri M, Huld TA, Dunlop ED. PV-GIS: a web-based solar radiation database for the calculation of PV potential in Europe. International Journal of Sustainable Energy 2005; 24:55–67.

[29] Hofierka J, Kaňuk J. Assessment of photovoltaic potential in urban areas using open-source solar radiation tools. Renewable Energy 2009; 34:2206–2214.

[30] Miguet F, Groleau D. Simulation tool including transmitted direct and diffuse light: application to the evaluation of daylighting inside glazed intermediate spaces. In: Proceedings of the 7th IBPSA 2001; 907–914.

[31] Mardaljevic J. Simulation of annual daylighting profiles for internal illuminance. Lighting Research and Technology 2000; 32:111–118.

[32] Compagnon R. Solar and daylight availability in the urban fabric. Energy and Buildings 2004; 36:321–328.

[33] Robinson D. Urban morphology and indicators of radiation availability. Solar Energy 2006; 80:1643–1648.

[34] Ward GJ. The RADIANCE lighting simulation and rendering system. In: Proceedings of the 21st annual conference on Computer graphics and interactive techniques – SIGGRAPH '94 1994; 459–472.

[35] Laua KKL, Lindberg F, Johansson E, Rasmussen MI, Thorsson S. Investigating solar energy potential in tropical urban environment: Acase study of Dar es Salaam, Tanzania. Sustainable Cities and Society 2017; 30:118–127.

[36] Takebayashi H, Ishii E, Moriyama M, Sakaki A, Nakajima S, Ueda H. Study to examine the potential for solar energy utilization based on the relationship between urban morphology and solar radiation gain on building rooftops and wall surfaces. Solar Energy 2015; 119:362–369.

[37] Sarralde JJ, Quinn DJ, Wiesmann D, Steemers K. Solar energy and urban morphology: Scenarios for increasing the renewable energy potential of neighbourhoods in London. Renewable Energy 2015; 73:10–17.

[38] Martins TAL, Adolphe L, Bastos LEG, Martins MAL. Sensitivity analysis of urban morphology factors regarding solar energy potential of buildings in a Brazilian tropical context. Solar Energy 2016; 137:11–24.

[39] Aflaki A, Mirnezhad M, Ghaffarianhoseini A, Ghaffarianhoseini A, Omrany H, Wang ZH, Akbar H. Urban heat island mitigation strategies: A state-of-the-art review on Kuala Lumpur, Singapore and Hong Kong. Cities 2017; 62:131–145.

[40] Masson, V. *et al.* Solar panels reduce both global warming and urban heat island. Frontiers in Environmental Science 2014; 2:14.

[41] Anjomshoaa A, Duarte F, Rennings D, Matarazzo T, deSouza P, Ratti C. City Scanner: Building and Scheduling a Mobile Sensing Platform for Smart City Services. IEEE Internet of Things Journal 2008; 5:4567–4579.

[42] Hall A. Brighton gears up for new fleet of solar-powered buses, https://www.theguardian.com/sustainable-business/2016/oct/08/brighton-solar-powered-buses-electric; 2016 [accessed 19 July 2018].

[43] OSM Buildings. Free web viewer for 3D building geometry, https://osmbuildings.org/; 2019 [accessed 29 December 2018].

[44] NYC DoITT. NYC 3-D Building Model, https://www1.nyc.gov/site/doitt/initiatives/3d-building.page; 2019 [accessed 29 December 2018].

[45] Los Angeles County Enterprise GIS. Countywide Building Outlines–2008–Public Domain, https://egis3.lacounty.gov/dataportal/2011/04/28/countywide-building-outlines/; 2019 [accessed 29 December 2018].

[46] Hawaii Statewide GIS Program. Building Footprints (CCH), http://geoportal.hawaii.gov/datasets/cchnl::building-footprints-cch; 2019 [accessed 29 December 2018].

[47] City of Toronto. A geospatial 3D ESRI shape format file of building shapes for City of Toronto, https://www.toronto.ca/city-government/data-research-maps/open-data/open-data-catalogue/#db07630f-252d-f7ae-2dff-8d0b38ec6576; 2019 [accessed 29 December 2018].

[48] ArcGIS Hub. Building footprint of Chan Aye Thazan Township in Mandalay city, Myanmar, http://hub.arcgis.com/datasets/fe1f23ec246e4b78a57bc362aa61699c_0?geometry=96.032%2C21.962%2C96.158%2C21.99; 2019 [accessed 29 December 2018].

[49] Land Monitoring Service. Building height 2012, https://land.copernicus.eu/local/urban-atlas/building-height-2012/view; 2019 [accessed 29 December 2018].

[50] OpenStreetMap. A map of the world, created by people like you and free to use under an open license, https://www.openstreetmap.org; 2019 [accessed 29 December 2018].

[51] ArcGIS for Desktop. Points solar radiation, http://desktop.arcgis.com/en/arcmap/10.3/tools/spatial-analyst-toolbox/points-solar-radiation.htm; 2019 [accessed, 7 December 2018].

[52] World Weather Online. Historical monthly weather, https://www.worldweatheronline.com; 2019 [accessed 7 December 2018].

[53] Sun Earth Tools. Tools for consumers and designers of solar, https://www.sunearthtools.com/dp/tools/pos_sun.php?lang=en; 2019 [accessed, 7 December 2018].

[54] Salleh SA, Abd Latif Z, Pradhan B, Wan WMN, Chan A. Functional relation of land surface albedo with climatological variables: a review on remote sensing techniques and recent research developments. Geocarto International 2013; 29:147–163.

[55] Yaghoobian N, Kleissl J. Effect of reflective pavements on building energy use. Urban Climate 2012; 2:25–42.